Past and future decline of tropical pelagic biodiversity

Moriaki Yasuhara (安原盛明)[a,b,1,2], Chih-Lin Wei[c,1], Michal Kucera[d,e], Mark J. Costello[f,g], Derek P. Tittensor[h,i], Wolfgang Kiessling[j], Timothy C. Bonebrake[b], Clay R. Tabor[k], Ran Feng[k], Andrés Baselga[l,m], Kerstin Kretschmer[d,e], Buntarou Kusumoto[n], and Yasuhiro Kubota (久保田康裕)[n]

[a]Swire Institute of Marine Science, The University of Hong Kong, Hong Kong Special Administrative Region, China; [b]School of Biological Sciences, The University of Hong Kong, Hong Kong Special Administrative Region, China; [c]Institute of Oceanography, National Taiwan University, 106 Taipei, Taiwan; [d]MARUM–Center for Marine Environmental Sciences, University of Bremen, 28359 Bremen, Germany; [e]Faculty of Geosciences, University of Bremen, 28359 Bremen, Germany; [f]School of Environment, The University of Auckland, 1142 Auckland, New Zealand; [g]Faculty of Biosciences and Aquaculture, Nord University, 8049 Bodø, Norway; [h]Department of Biology, Dalhousie University, Halifax, NS, B3H 4R2 Canada; [i]United Nations Environment Programme World Conservation Monitoring Centre, CB3 0DL Cambridge, United Kingdom; [j]GeoZentrum Nordbayern, Department of Geography and Geosciences, Friedrich-Alexander Universität Erlangen–Nürnberg, 91054 Erlangen, Germany; [k]Department of Geosciences, University of Connecticut, Storrs, CT 06269; [l]Departamento de Zoología, Genética y Antropología Física, Facultad de Biología, Universidad de Santiago de Compostela, 15782 Santiago de Compostela, Spain; [m]CRETUS Institute, Universidad de Santiago de Compostela, 15782 Santiago de Compostela, Spain; and [n]Faculty of Science, University of the Ryukyus, 903-0213 Okinawa, Japan

Edited by James P. Kennett, University of California, Santa Barbara, CA, and approved April 15, 2020 (received for review October 1, 2019)

A major research question concerning global pelagic biodiversity remains unanswered: when did the apparent tropical biodiversity depression (i.e., bimodality of latitudinal diversity gradient [LDG]) begin? The bimodal LDG may be a consequence of recent ocean warming or of deep-time evolutionary speciation and extinction processes. Using rich fossil datasets of planktonic foraminifers, we show here that a unimodal (or only weakly bimodal) diversity gradient, with a plateau in the tropics, occurred during the last ice age and has since then developed into a bimodal gradient through species distribution shifts driven by postglacial ocean warming. The bimodal LDG likely emerged before the Anthropocene and industrialization, and perhaps ∼15,000 y ago, indicating a strong environmental control of tropical diversity even before the start of anthropogenic warming. However, our model projections suggest that future anthropogenic warming further diminishes tropical pelagic diversity to a level not seen in millions of years.

latitudinal diversity gradients | planktonic foraminifera | temperature | Last Glacial Maximum | climate change

Latitudinal diversity gradients (LDGs), the equatorially centered parabolic diversity patterns, have been described for over 200 y in terrestrial systems (1–4) and are also well established in marine environments (5–7). However, there is an increasing recognition that marine LDGs, particularly those in open-ocean systems, tend to have an tropical diversity depression and thus, to be bimodal (8–14).

This current tropical depression is consistent with present-day temperatures being beyond the upper physiological thermal tolerances of some species. An inability of species to tolerate high temperatures or sustained physiological stresses may cause shifts of their latitudinal ranges farther poleward as the climate warms. Indeed, a near-future tropical biodiversity decline has been predicted with ongoing human-induced climate warming (15–19), and ecosystem-scale impacts of ocean warming are already evident (20–24).

Alternatively, or additionally, the current tropical dip in diversity could be explained through an evolutionary mechanism of higher speciation rates and/or lower extinction rates at the edges of the tropics (8, 13). Distinguishing the ecological and evolutionary timescale processes responsible for observed variations in the shape of marine LDGs is critical for assessing the outcome of biotic responses to rapid anthropogenic warming over the coming century (12). However, the lack of a standardized paleoecological baseline for the pelagic LDG has compromised separating whether the observed bimodality is caused by a rapid ecological response to ocean warming, by a longer-term and slower evolutionary process, or both (e.g., ref. 14). While several paleontological studies have shown bimodal LDGs (25), they are not directly comparable with the present-day pelagic bimodality or do not answer this question directly, because they are terrestrial, not global in extent, or too deep time (e.g., Paleogene or Mesozoic) to evaluate the hypothesis of rapid ecological response.

The calcified shells of planktonic foraminifers, abundant and widespread protists in the world's oceans, are well preserved in marine sediments and can thus provide a baseline for tracking trends in the LDG over the geologic past (26, 27). In addition, the relationship between temperature and planktonic foraminiferal diversity is consistent with that of many other open-ocean organisms (5, 11, 28). Here, we use global datasets of pre-industrial (broadly representing a Late Holocene situation) (*Materials and Methods*) and Last Glacial Maximum (LGM; ca. 21 ky ago) planktonic foraminifers as well as a future diversity projection to provide empirical evidence that the tropical diversity depression is neither a recent anthropogenic phenomenon nor of deep-time origin. Rather, it was likely caused by a post–ice-age warming, suggesting a major role for distributional shifts driven by climate.

Results and Discussion

Diversity Patterns with Latitude and Temperature. Our global analysis of planktonic foraminiferal diversity (calculated as species richness [Hill number, $q = 0$] and effective number of common species [Hill number, $q = 1$]) (*Materials and Methods*)

Significance

We discovered that the tropical oceanic diversity depression is not a recent phenomenon nor very deep time in origin by using a comprehensive global dataset of the calcified shells of planktonic foraminifers, abundant unicellular organisms in the world's oceans, which are exceptionally well preserved in marine sediments as fossils. The diversity decline in the lowest latitudes may have started due to rapid post–ice-age warming around 15,000 y ago. Warming may by the end of this century diminish tropical oceanic diversity to an unprecedented level in human history.

Author contributions: M.Y. designed research; M.Y., C.-L.W., M.K., M.J.C., D.P.T., W.K., T.C.B., C.T., R.F., A.B., K.K., B.K., and Y.K. performed research; M.Y., C.-L.W., and D.P.T. analyzed data; and M.Y., C.-L.W., M.K., M.J.C., D.P.T., W.K., T.C.B., C.T., R.F., A.B., K.K., B.K., and Y.K. wrote the paper.

The authors declare no competing interest.

This article is a PNAS Direct Submission.

[1]M.Y. and C.-L.W. contributed equally to this work.

[2]To whom correspondence may be addressed. Email: moriakiyasuhara@gmail.com.

This article contains supporting information online at https://www.pnas.org/lookup/suppl/doi:10.1073/pnas.1916923117/-/DCSupplemental.

First published May 26, 2020.

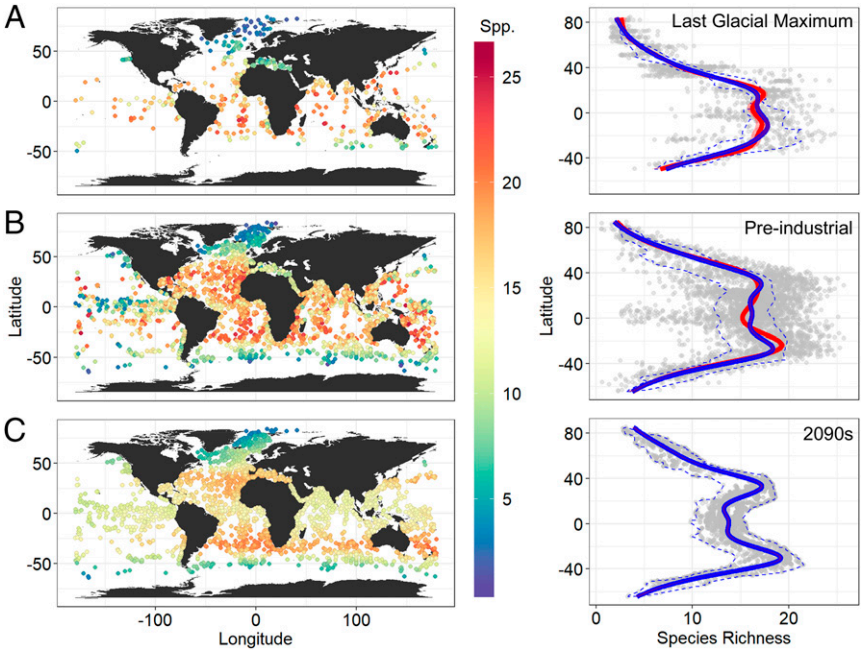

Fig. 1. Species richness of planktonic foraminifers during the (*A*) LGM, (*B*) PIC, and for (*C*) 2091 to 2100 (2090s) as maps and latitudinal gradients. Colored and gray dots (in the maps and the latitudinal gradients, respectively) indicate the observed diversities in *A* (LGM) and *B* (PIC). These observed LGM and PIC diversities were modeled by SST, coordinates, and ocean basin using a GAM to predict the diversities in 2090s (colored and gray dots in *C*) with future SST (based on RCP 8.5) as well as those during the LGM and PIC themselves. The predicted latitudinal diversities for the three time periods (enclosed by blue dashed lines) were smoothed by a GAM to show LDGs (blue lines). The latitudinal gradients of observed diversities during the LGM and PIC were also fitted by a GAM and shown as the red lines with the shaded areas indicating the 95% CIs (the shaded area is small, overlaps the red line, and so is not visible in the PIC panel). For the LGM and PIC gray dots, a small amount of jitter was added on the *x* axis to make them visible when overlapping. *SI Appendix*, Fig. S1 shows empirical and projected diversities using a Hill number of order $q = 1$.

demonstrates that during the LGM, the LDG was unimodal (or only weakly bimodal), whereas the preindustrial LDG was bimodal with a distinct tropical diversity depression (Fig. 1 and *SI Appendix*, Fig. S1 and Tables S1 and S2). This indicates that the strength of the bimodal LDG for planktonic foraminifers cannot be entirely due to long-term evolutionary processes because it was minimal during the LGM (Fig. 1 and *SI Appendix*, Fig. S1 and Tables S1 and S2), and there have been no known global extinctions or speciations of any planktonic foraminiferal species since the LGM (29).

We propose that the cause of the bimodality may then be environmentally driven extirpation and/or immigration. During warming, any diversity losses at higher latitudes (due to range shifts of species to even higher latitudes) are compensated for by the poleward movements of species from lower latitudes. However, in the tropics, such compensation due to species range shifts is not possible, resulting in a tropical diversity decline (15, 17, 30, 31).

It is unlikely that the tropical diversity depression is a very recent phenomenon originating in the Anthropocene because we found that the preindustrial LDG was already bimodal. Thus, the bimodal LDG most likely developed during the post-LGM warming, with a 5.2% loss in the mean projected species richness since the LGM at the equator (calculated based on the mean predictions within ±1° latitude) (Fig. 1).

The LDG exhibited a tropical plateau (or weak bimodality) during the LGM (Fig. 1 and *SI Appendix*, Fig. S1) indicating an approach toward diversity saturation (at or beyond the optimum in the unimodal temperature–diversity relationship; see the next paragraph) with relatively low maximum global sea temperature. The distinct tropical diversity decline may have begun ∼15,000 y ago, given that a rapid postglacial warming started at that time (32). The duration of glacial periods has been much longer than that of interglacial periods during the Late Quaternary. Therefore, the tropical thermal niches of marine organisms may be optimized to the maximum temperatures of glacial periods, leading to tropical diversity depressions during warm periods, given that marine niche conservatism is known to have existed during Late Quaternary climate changes (33). As a bimodal LDG is known to be present during the last interglacial (in corals) (34), it is likely that the bimodal LDG has appeared repeatedly during warm interglacial periods during the Late Quaternary and weakened during glacial periods. Species adapted to very warm temperatures existed during the Pliocene, the major previous warmer-than-present period, but significant extinctions of these species are known during the Plio–Pleistocene cooling (27). Note that pre-Plio–Pleistocene Phanerozoic LDGs are also known to be dynamic (14, 35–37), although the underlying mechanism may be different.

Sea surface temperature (SST) has been and is unimodal with latitude (Fig. 2*D*) (the next paragraph discusses the equatorial upwelling zone). It is also predicted to remain unimodal under the RCP 8.5 "business-as-usual" climate warming scenario in 2091 to 2100 ("2090s" hereafter), with ∼0 to 4 °C warming relative to the preindustrial control (PIC) (Fig. 2). The magnitude of the predicted warming from the PIC to the RCP 8.5 2090s will be larger (and much more rapid) than that from the LGM to PIC (Fig. 2), particularly in the tropics. The unimodal (or only weakly bimodal) LDG during the LGM and the bimodal LDG during the preindustrial time period reflect a positive temperature–diversity relationship from −2 to 20 °C and a negative relationship beyond that, especially beyond 25 °C and for species richness (*SI Appendix*, Fig. S2). Thus, the present reduction of species diversity in the tropics is likely due to high sea temperatures (*SI Appendix*, Fig. S2), a thermal response also identified in other pelagic groups (38). Such very high mean temperatures (those exceeding 25 °C) did not exist in any latitudinal band during the LGM (Fig. 2). Supporting our interpretation is the observation that planktonic foraminifer species tend to have optimum temperature

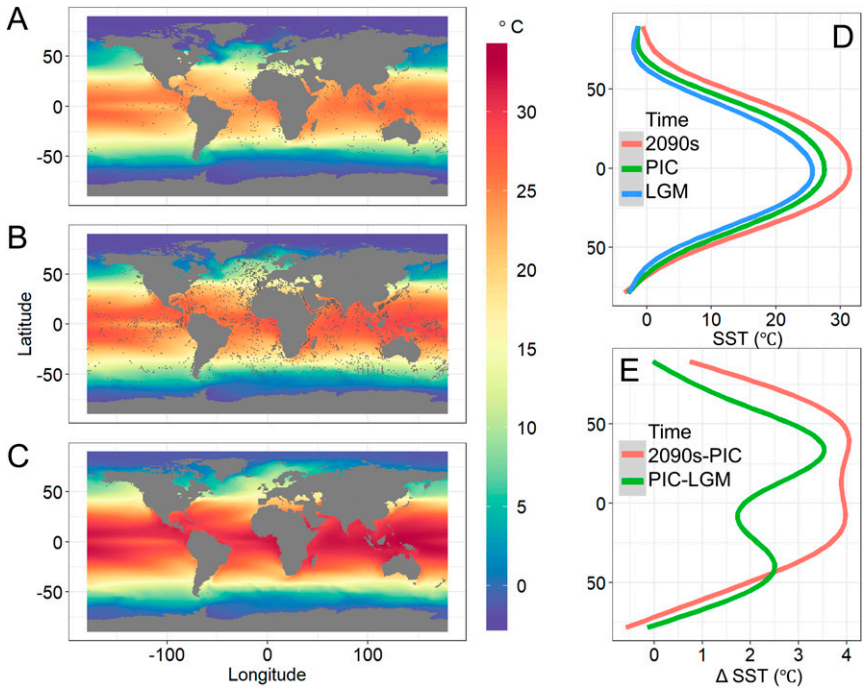

Fig. 2. Maps and latitudinal gradients of the projected ocean SST during the (*A*) LGM, (*B*) PIC, and (*C*) 2091 to 2100 (2090s) based on RCP 8.5. The latitudinal SST (LGM: blue; PIC: green; 2090s: red) and ΔSST (warming from the LGM to PIC as green and from the PIC to 2090s as red) are smoothed by a GAM and shown in *D* and *E*, respectively. Gray dots in *A* and *B* indicate sample locations.

ranges at ∼20 to 30 °C, with a sharp drop in their growth rates above these temperatures, showing a high-end temperature threshold of thermal performance curves (19, 39, 40). Using the relationship between SST and diversity for both time periods (LGM and PIC), we predict a more than 15% diversity loss at the equator (calculated based on the mean predictions within ±1° latitude) within this century under the business-as-usual climate warming scenario (Fig. 1 and *SI Appendix*, Fig. S1). In comparison, only ∼5% diversity loss at the equator has been observed between the LGM and PIC (Fig. 1 and *SI Appendix*, Fig. S1), indicating the potential for a three times greater reduction over the coming century. It is also noteworthy that corals had a bimodal LDG in the last interglacial, a warmer-than-present time period (34). Thus, we may see tropical diversity decline not only in planktonic foraminifers but also in other taxonomic and functional groups with further future warming.

In the equatorial upwelling zone of the eastern Pacific Ocean (especially at ∼100 to 120°W) (Fig. 2*B*), SST is lower than that in adjacent higher-latitude (e.g., 5 to 10°N and S) tropical waters, which may affect species diversity. Indeed, the equatorial diversity is higher than that at 5 to 10°N and S in the eastern Pacific at ∼100 to 120°W (Fig. 1*B*). Thus, in the present-day ocean, the equatorial upwelling zone with lower temperature than adjacent higher-latitude tropical waters may be within or close to the optimum temperature range of many species and act as a refugium. In the future warmer ocean, however, temperature will be beyond the optimum temperature range even in the equatorial upwelling zone (Fig. 2*C*), and the refugium will disappear (Fig. 1*C*). Nonetheless, the equatorial upwelling zone does not affect our major results because the low temperature zone related to the equatorial upwelling is limited to a very narrow equatorial band of the eastern Pacific Ocean. The analyses of just the Atlantic Ocean, which lacks

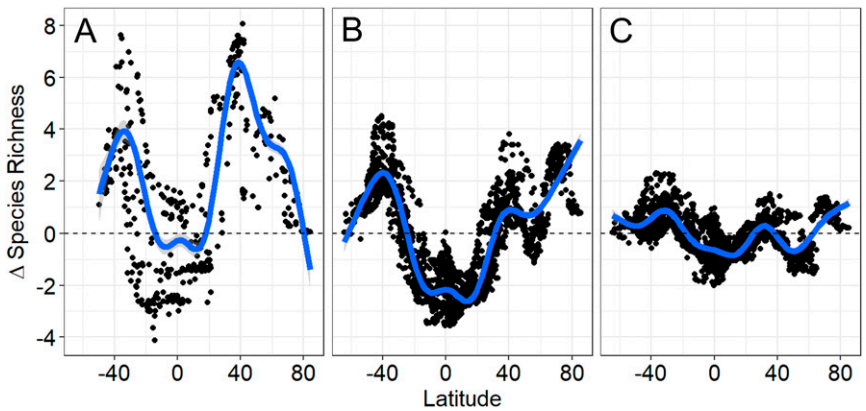

Fig. 3. Changes in predicted species richness (Δ species richness) from the LGM to PIC (*A*), from the PIC to RCP 8.5 2090s (*B*), and from the PIC to RCP 2.6 2090s (*C*). Species richness was predicted using SST for LGM, PIC, RCP 8.5 2090s, and RCP 2.6 2090s. The Δ species richness was calculated for the LGM samples in *A* and PIC samples in *B* and *C* and smoothed by a GAM (blue lines with the gray shaded areas indicating the 95% CIs that are small and not visible in *B* and *C*).

a distinct equatorial temperature decline, show the same basic results (*Materials and Methods*).

Higher-latitude, especially temperate, diversity increases from the LGM to PIC and from the PIC to RCP 8.5 2090s and offsets the tropical diversity decline (Fig. 3). The temperate peaks of diversity shift poleward in the comparison between the PIC and RCP 8.5 2090s (Fig. 3*B*) relative to that between the LGM and PIC (Fig. 3*A*), indicating that future warming will further enhance poleward species range shifts. Both the tropical diversity decline and temperate diversity increase from the PIC to 2090s would be reduced with the low-emission scenario RCP 2.6 relative to the business-as-usual scenario RCP 8.5 (Fig. 3*C*). The subpolar diversity decline from the PIC to 2090s (negative Δ diversity peak at ~50 to 60°N) (Fig. 3 *B* and *C*) is probably due to projected subpolar North Atlantic cooling related to a collapse of the local deep-ocean convection (41–43).

Beta Diversity and the Process of Diversity Change. Beta diversity quantifies how species composition changes in space and time: for example, in response to temperature gradients and ocean warming. We divided beta diversity into turnover and nestedness components (Fig. 4 and *Materials and Methods*). Turnover occurs with species replacement along an environmental gradient, and nestedness indicates species loss without replacement (i.e., when an assemblage is a subset of a more species-rich neighboring biota). The relative contributions of turnover and nestedness components had positive and negative peaks, respectively, in the tropics during the LGM, showing unimodal and inverse unimodal LDGs (Fig. 4). Since then, the peaks have moved poleward toward the edges of the tropics, showing bimodal and inverse bimodal LDGs during the preindustrial time (Fig. 4). The tropical peak of the preindustrial inverse bimodal nestedness LDG is due to a reduction of species, presumably those most sensitive to the warming. In other words, the preindustrial tropical assemblage has lost species and has become more of a subset of the adjacent higher-latitude tropical assemblages. The peaks in relative contribution of turnover (positive) and nestedness (negative) to beta diversity at the edges of the preindustrial tropics (Fig. 4) indicate distributional shifts of some of tropical species, which had an equatorial distribution during the LGM, toward higher latitudes (*SI Appendix*, Fig. S3). Overall, 23 of 27 species extended their interquartile range (75 to 25 percentiles) and shifted southern and northern edges of distributions (97.5 to 2.5 percentiles) poleward since the LGM, and 6 of 27 species show much stronger bimodal latitudinal distributions of their occurrence density in the PIC than in the LGM, which is probably responsible for the observed bimodal PIC LDG (*SI Appendix*, Fig. S3).

Future Scenario. A future tropical diversity depression has not only been predicted for planktonic foraminifers but also for other taxonomic and functional groups (Fig. 1) (8, 9, 11, 18, 19). Planktonic foraminifer diversity is known to track marine and especially pelagic diversity (5, 26). Given the exceptional fossil record of planktonic foraminifers used here as an ideal model system (26, 44) and the fact that most marine organisms have poor fossil records, our findings may further apply to other taxonomic groups. For example, Kaschner et al. (45) suggested a reduction of tropical and an increase in temperate diversity in marine mammals under a warming scenario.

In a warmer pelagic world, temperate regions will hold more tropical species, and polar regions more temperate species, as they change their distributions to live within their optimum temperature niches (16). However, tropical regions will have no source for such immigrants (16–18). Our study shows that this tropical dead end causes a local diversity reduction of planktonic foraminifers between 20°S and N. The situation will worsen with continued global warming in the coming decades, particularly without appropriate mitigation of greenhouse gas emissions (Fig. 3). This tropical pelagic diversity decline likely emerged before industrialization and the Anthropocene and perhaps during

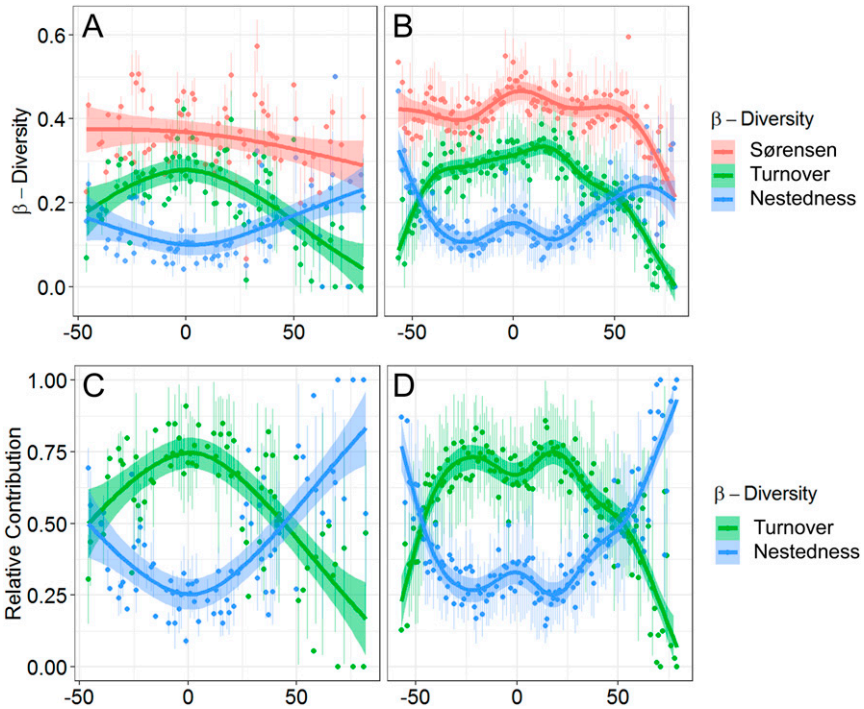

Fig. 4. The latitudinal gradients in beta diversity during (*A*) the LGM and (*B*) the preindustrial periods. The total beta diversity (i.e., Sørensen dissimilarity [red]) was separated into turnover (green) and nestedness (blue) components. *C* and *D* show the relative contribution of the turnover (green) and nestedness (blue) components to total dissimilarity for the LGM and preindustrial periods, respectively. Colored dots and error bars show mean and SD from 1,000 bootstrap resampling within a 1° moving window. Colored lines with shaded areas show GAM fit to the mean values and 95% CI.

the onset of the postglacial warming ~15,000 y ago. Future anthropogenic warming may diminish tropical diversity to a level not seen in millions of years.

Materials and Methods

Foraminifera. We used exceptionally comprehensive global census datasets of planktonic foraminifera, the ForCenS (46) and the MARGO (47, 48) compilations, for "present-day" preindustrial (below) and LGM LDG reconstructions, respectively. The databases comprise specimens collected using a constant 150-μm sieve size [Yasuhara et al. (27) has a discussion on the sieve size]. We consider *Globigerinoides ruber* pink and white as separate species. We merged *Globorotalia menardii* and *Globorotalia tumida*. P/D integrade is merged with *Neogloboquadrina incompta*. Otherwise, we used species only and did not use subspecies or categories including multiple species. *Globorotalia crassula* was removed from the datasets because it already became extinct ~0.9 million y ago (28, 29). We also removed small, rare, and/or taxonomically obscure species (*Tenuitella iota*, *Berggrenia pumilio*, *Dentigloborotalia anfracta*, *Globorotalia cavernula*, *Globigerinita minuta*, and *Globorotalia ungulata*) following Siccha and Kucera (46). Eventually, we used these 34 species: *Beella digitata*, *Candeina nitida*, *Globigerina bulloides*, *Globigerina falconensis*, *Globigerinella adamsi*, *Globigerinella calida*, *Globigerinella siphonifera*, *Globigerinita glutinata*, *Globigerinita uvula*, *Globigerinoides conglobatus*, *G. ruber* pink, *G. ruber* white, *Globigerinoides tenellus*, *Globoconella inflata*, *Globoquadrina conglomerata*, *Globorotalia crassaformis*, *Globorotalia hirsuta*, *G. menardii + tumida*, *Globorotalia scitula*, *Globorotalia theyeri*, *Globorotalia truncatulinoides*, *Globorotaloides hexagonus*, *Globoturborotalita rubescens*, *Hastigerina pelagica*, *Hastigerinella digitata*, *Neogloboquadrina dutertrei*, *N. incompta*, *Neogloboquadrina pachyderma*, *Orbulina universa*, *Pulleniatina obliquiloculata*, *Sphaeroidinella dehiscens*, *Trilobatus sacculifer*, *Turborotalita humilis*, and *Turborotalita quinqueloba*. After removing duplicated samples, the preindustrial ForCenS and LGM MARGO datasets include 4,138 and 1,442 samples, respectively, with >~300 specimens per sample for most samples (46–48). Given generally slow sedimentation rate in the deep sea, the ForCenS core top present-day dataset probably represents mostly the Late Holocene (= the last few thousand years) but preindustrial and pre-Anthropocene (49). Although a small proportion of specimens would be from the Anthropocene, they should be negligible, given time averaging of a few thousand years. It is unlikely that the bimodal LDGs are artifacts of sampling biases (50) because tropical regions are well sampled in our datasets (Fig. 1 and *SI Appendix*, Fig. S1), and the less sampled LGM dataset does not show a remarkably bimodal LDG.

Temperature. We used the three-dimensional, fully coupled Earth system models from the Goddard Institute for Space Studies, IPSL-CM5A-LR from the Institut Pierre Simon Laplace (GISS-E2-R), and from the Max Planck Institute (MPI-ESM-P) to calculate the ensemble average of annual mean SST for the last 100 y during the LGM (51–53). For the last 100 y of the PIC scenario and the years 2091 to 2100 (2090s) projections (RCP, Representative Concentration Pathway, 8.5 also known as business-as-usual scenario and RCP 2.6 with appropriate mitigations of carbon dioxide emission), we use Earth system model simulations from the Geophysical Fluid Dynamics Laboratory (GFDL-ESM-2G), the Institut Pierre Simon Laplace (IPSL-CM5A-MR), and the Max Planck Institute (MPI-ESM-MR) to calculate the ensemble average of the annual mean SST (52, 54, 55). We reprojected the SST layer of each Earth system model to 0.5 by 0.5° grids based on bilinear interpolation and then calculated the multimodel average of each interpolated grid. All Earth system models are part of the Coupled Model Intercomparison Project Phase 5 and were downloaded from the Earth System Grid Federation Peer-to-Peer enterprise system (https://esgf.llnl.gov/).

Statistical Modeling. For diversity measures, we used Hill numbers (56), ${}^qD = \left(\sum_{i=1}^{S} p_i^q\right)^{1/(1-q)}$, where S is the number of species in a site and p_i is the relative abundance of the ith species. The (larger) value of order q discounts the rare species and thus, emphasizes the abundant species. When $q = 0$, all species have equal weight, and ${}^qD$ is equivalent to species richness. Where q approaches one, the derived mathematical expression of Hill numbers (${}^1D$) is given as ${}^1D = \exp\left(-\sum_{i=1}^{S} p_i^q \log(p_i)\right)$. Because the equation gives more weight to common species (with higher relative abundance), it can be interpreted as the effective number of equally abundant and common (typical) species in a community (57). Both measures were very similar in our results, so we present the Hill number of order $q = 0$ in the text because species richness is the most intuitive and commonly used measure of diversity and $q = 1$ (the exponential form of the Shannon index) in *SI Appendix*.

We decomposed beta diversity (multiple-site Sørensen dissimilarity), which is influenced by turnover and species richness, into spatial turnover (also called Simpson's dissimilarity index) and nestedness components (58, 59). The beta-diversity measures and partitions were conducted over a 1° latitude moving window. Within each moving window, five sites were randomly resampled (with replacement) for 1,000 times to estimate the mean and SD. Windows with less than five sites were omitted from the calculations. The same analyses were tested across 1 to 5° latitude moving windows and show consistent latitudinal patterns in beta diversity (*SI Appendix*, Fig. S4).

The latitudinal gradients of diversity were fitted by a generalized additive model (GAM) with a quasi-Poisson error distribution and a thin plate regression spline for the LGM and PIC datasets. We also used a GAM to fit the LGM or PIC SST to their observed Hill numbers (e.g., species richness or effective number of common species) to visualize the thermal gradient of diversity. Finally, we constructed a third type of GAM using SST, longitude, latitude (and their interaction), the ocean basins (i.e., Atlantic, Pacific, Indian, Arctic, and Southern Oceans) where the samples were collected, and time (LGM and PIC) as predictor variables to account for spatial and temporal diversity variations and to project the future distribution of species richness based on the ensemble average of projected SST under RCP 8.5 and RCP 2.6 in the 2090s. The basis dimensions in the GAMs was chosen ($k = 5$ or 6) to generate smooth curve fit for ease of interpretation; nevertheless, the fitted lines in general agree to the GAM with automatic selection of k.

All statistical analyses were performed with R version 3.5.1 (60). Hill numbers and multivariate analysis used the vegan package (61); beta diversity used the betapart package (62); GAMs used the mgcv package (63); and GIS (geographic information system) mapping and data visualization used the raster, sp, and ggplot2 packages (64–66). A significance level of $\alpha = 0.05$ was applied to all statistical tests. All model residuals were checked by standard diagnostic plots (i.e., residual vs. fitted values, quantile-quantile plot) for assumptions of homogeneity, independence, and normal distribution and by Moran's I test, Moran's I spatial correlogram, and variogram for spatial autocorrelation (67). The assumptions of homogeneity, independence, and normal distribution were reasonably met. Spatial autocorrelations in the model residuals were detected at distances up to 2,791 km for the LGM and 1,696 km for PIC species richness (Hill numbers of order $q = 0$) and up to 785 km for the LGM and 1,229 km for PIC effective number of common species (Hill numbers of order $q = 1$).

Dissolution of planktonic foraminiferal shells and upwelling may affect diversity. To demonstrate that the diversity patterns were not affected by dissolution or upwelling, we ran the same analysis for three subsets, namely samples with water depth less than 3,000 m, those from the Atlantic Ocean only, and those excluding all coastal ecoregions and thus, coastal upwelling areas (68). The shallow-depths and Atlantic subsets have higher calcium carbonate saturation state and thus, better foraminiferal preservation (than the whole dataset including deeper depths and other oceans than the Atlantic). The Atlantic Ocean does not have a distinct low-temperature zone related to the equatorial upwelling, compared with the Pacific Ocean (Fig. 2). The results of these subsets remain qualitatively the same (*SI Appendix*, Figs. S5–S7), showing that our results are not artifacts of preservation or affected by upwelling.

Data and Materials Availability. All data are available in the text, *SI Appendix*, and Dryad (https://doi.org/10.5061/dryad.g1jwstqnn).

ACKNOWLEDGMENTS. We thank Michael Siccha for helping with the foraminiferal dataset and the editors and three anonymous reviewers for constructive comments. This project is supported by bioDISCOVERY, Future Earth. The work described in this paper was partially supported by Research Grants Council of the Hong Kong Special Administrative Region, China, Projects HKU 17302518, HKU 17303115, and HKU 17311316; Seed Funding Programme for Basic Research of the University of Hong Kong, Projects 201611159053 and 201711159057; Faculty of Science RAE Improvement Fund of the University of Hong Kong (to M.Y.); Ministry of Science Technology Taiwan, Project 108-2611-M-002-001 (to C.-L.W.); the Program for Advancing Strategic International Networks to Accelerate the Circulation of Talented Researchers, the Japan Society for the Promotion of Science (to Y.K.); Deutsche Forschungsgemeinschaft, Projects KI 806/16-1 and FOR 2332 (to W.K.); Deutsche Forschungsgemeinschaft, Germany's Excellence Strategy, EXC-2077, Project 390741603 (to M.K.); and the Jarislowsky Foundation (to D.P.T.).

1. T. C. Bonebrake, Conservation implications of adaptation to tropical climates from a historical perspective. *J. Biogeogr.* **40**, 409–414 (2013).
2. P. V. A. Fine, Ecological and evolutionary drivers of geographic variation in species diversity. *Annu. Rev. Ecol. Evol. Syst.* **46**, 369–392 (2015).
3. H. Hillebrand, On the generality of the latitudinal diversity gradient. *Am. Nat.* **163**, 192–211 (2004).
4. M. R. Willig, D. M. Kaufman, R. D. Stevens, Latitudinal gradients of biodiversity: Pattern, process, scale, and synthesis. *Annu. Rev. Ecol. Evol. Syst.* **34**, 273–309 (2003).
5. D. P. Tittensor *et al*., Global patterns and predictors of marine biodiversity across taxa. *Nature* **466**, 1098–1101 (2010).
6. G. Beaugrand, I. Rombouts, R. R. Kirby, Towards an understanding of the pattern of biodiversity in the oceans. *Glob. Ecol. Biogeogr.* **22**, 440–449 (2013).
7. H. Hillebrand, Strength, slope and variability of marine latitudinal gradients. *Mar. Ecol. Prog. Ser.* **273**, 251–267 (2004).
8. C. Chaudhary, H. Saeedi, M. J. Costello, Bimodality of latitudinal gradients in marine species richness. *Trends Ecol. Evol.* **31**, 670–676 (2016).
9. C. Chaudhary, H. Saeedi, M. J. Costello, Marine species richness is bimodal with latitude: A reply to Fernandez and Marques. *Trends Ecol. Evol.* **32**, 234–237 (2017).
10. H. Saeedi, T. E. Dennis, M. J. Costello, Bimodal latitudinal species richness and high endemicity of razor clams (*Mollusca*). *J. Biogeogr.* **44**, 592–604 (2017).
11. S. Rutherford, S. D'Hondt, W. Prell, Environmental controls on the geographic distribution of zooplankton diversity. *Nature* **400**, 749–753 (1999).
12. B. Worm, D. P. Tittensor, *A Theory of Global Biodiversity* (Princeton University Press, Princeton, NJ, 2018).
13. A. Brayard, G. Escarguel, H. Bucher, Latitudinal gradient of taxonomic richness: Combined outcome of temperature and geographic mid-domains effects? *J. Zool. Syst. Evol. Res.* **43**, 178–188 (2005).
14. M. G. Powell, V. P. Beresford, B. A. Colaianne, The latitudinal position of peak marine diversity in living and fossil biotas. *J. Biogeogr.* **39**, 1687–1694 (2012).
15. G. Beaugrand, M. Edwards, V. Raybaud, E. Goberville, R. R. Kirby, Future vulnerability of marine biodiversity compared with contemporary and past changes. *Nat. Clim. Chang.* **5**, 695–701 (2015).
16. W. W. L. Cheung, D. Pauly, "Impacts and effects of ocean warming on marine fishes" in *Explaining Ocean Warming: Causes, Scale, Effects and Consequences*, D. Laffoley, J. M. Baxter, Eds. (IUCN, Gland, Switzerland, 2016), pp. 239–253.
17. W. W. L. Cheung, R. Watson, D. Pauly, Signature of ocean warming in global fisheries catch. *Nature* **497**, 365–368 (2013).
18. J. García Molinos *et al*., Climate velocity and the future global redistribution of marine biodiversity. *Nat. Clim. Chang.* **6**, 83–88 (2016).
19. T. Roy, F. Lombard, L. Bopp, M. Gehlen, Projected impacts of climate change and ocean acidification on the global biogeography of planktonic Foraminifera. *Biogeosciences* **12**, 2873–2889 (2015).
20. G. T. Pecl *et al*., Biodiversity redistribution under climate change: Impacts on ecosystems and human well-being. *Science* **355**, eaai9214 (2017).
21. T. Wernberg *et al*., Climate-driven regime shift of a temperate marine ecosystem. *Science* **353**, 169–172 (2016).
22. E. S. Poloczanska *et al*., Global imprint of climate change on marine life. *Nat. Clim. Chang.* **3**, 919–925 (2013).
23. T. D. Ainsworth *et al*., Climate change disables coral bleaching protection on the Great Barrier Reef. *Science* **352**, 338–342 (2016).
24. D. B. Field, T. R. Baumgartner, C. D. Charles, V. Ferreira-Bartrina, M. D. Ohman, Planktonic foraminifera of the California Current reflect 20th-century warming. *Science* **311**, 63–66 (2006).
25. P. D. Mannion, P. Upchurch, R. B. J. Benson, A. Goswami, The latitudinal biodiversity gradient through deep time. *Trends Ecol. Evol.* **29**, 42–50 (2014).
26. M. Yasuhara, D. P. Tittensor, H. Hillebrand, B. Worm, Combining marine macroecology and palaeoecology in understanding biodiversity: Microfossils as a model. *Biol. Rev.* **92**, 199–215 (2017).
27. M. Yasuhara, G. Hunt, H. J. Dowsett, M. M. Robinson, D. K. Stoll, Latitudinal species diversity gradient of marine zooplankton for the last three million years. *Ecol. Lett.* **15**, 1174–1179 (2012).
28. I. S. Fenton, P. N. Pearson, T. D. Jones, A. Purvis, Environmental predictors of diversity in recent planktonic foraminifera as recorded in marine sediments. *PLoS One* **11**, e0165522 (2016).
29. T. Aze *et al*., A phylogeny of Cenozoic macroperforate planktonic foraminifera from fossil data. *Biol. Rev.* **86**, 900–927 (2011).
30. M. T. Burrows *et al*., Geographical limits to species-range shifts are suggested by climate velocity. *Nature* **507**, 492–495 (2014).
31. J. M. Sunday, A. E. Bates, N. K. Dulvy, Thermal tolerance and the global redistribution of animals. *Nat. Clim. Chang.* **2**, 686–690 (2012).
32. K. K. Andersen *et al*.; North Greenland Ice Core Project members, High-resolution record of Northern Hemisphere climate extending into the last interglacial period. *Nature* **431**, 147–151 (2004).
33. A. M. Waterson, K. M. Edgar, D. N. Schmidt, P. J. Valdes, Quantifying the stability of planktic foraminiferal physical niches between the Holocene and Last Glacial Maximum. *Paleoceanography* **32**, 74–89 (2017).
34. W. Kiessling, C. Simpson, B. Beck, H. Mewis, J. M. Pandolfi, Equatorial decline of reef corals during the last Pleistocene interglacial. *Proc. Natl. Acad. Sci. U.S.A.* **109**, 21378–21383 (2012).
35. A. Boersma, I. Premoli Silva, Distribution of Paleogene planktonic foraminifera—analogies with the Recent? *Palaeogeogr. Palaeoclimatol. Palaeoecol.* **83**, 29–48 (1991).
36. I. S. Fenton *et al*., The impact of Cenozoic cooling on assemblage diversity in planktonic foraminifera. *Philos. Trans. R. Soc. Lond. B Biol. Sci.* **371**, 20150224 (2016).
37. M. G. Powell, The latitudinal diversity gradient of brachiopods over the past 530 million years. *J. Geol.* **117**, 585–594 (2009).
38. D. G. Boyce, D. P. Tittensor, B. Worm, Effects of temperature on global patterns of tuna and billfish richness. *Mar. Ecol. Prog. Ser.* **355**, 267–276 (2008).
39. F. Lombard, L. Labeyrie, E. Michel, H. J. Spero, D. W. Lea, Modelling the temperature dependent growth rates of planktic foraminifera. *Mar. Micropaleontol.* **70**, 1–7 (2009).
40. S. Žarić, B. Donner, G. Fischer, S. Mulitza, G. Wefer, Sensitivity of planktic foraminifera to sea surface temperature and export production as derived from sediment trap data. *Mar. Micropaleontol.* **55**, 75–105 (2005).
41. G. Sgubin, D. Swingedouw, S. Drijfhout, Y. Mary, A. Bennabi, Abrupt cooling over the North Atlantic in modern climate models. *Nat. Commun.*, 10.1038/ncomms14375 (2017). Erratum in: Nat. Commun. **9**, 16222 (2018).
42. S. Drijfhout, G. J. van Oldenbourgh, A. Cimatoribus, Is a decline of AMOC causing the warming hole above the North Atlantic in observed and modelled warming patterns? *J. Clim.* **25**, 8373–8379 (2012).
43. H. Kim, S. An, On the subarctic North Atlantic cooling due to global warming. *Theor. Appl. Climatol.* **114**, 9–19 (2013).
44. M. Yasuhara, Marine biodiversity in space and time: What tiny fossils tell. *Métode* **9**, 77–81 (2019).
45. K. Kaschner, D. P. Tittensor, J. Ready, T. Gerrodette, B. Worm, Current and future patterns of global marine mammal biodiversity. *PLoS One* **6**, e19653 (2011).
46. M. Siccha, M. Kucera, ForCenS, a curated database of planktonic foraminifera census counts in marine surface sediment samples. *Sci. Data* **4**, 170109 (2017).
47. M. Kucera, A. Rosell-Mele, R. Schneider, C. Waelbroeck, M. Weinelt, Multiproxy approach for the reconstruction of the glacial ocean surface (MARGO). *Quat. Sci. Rev.* **24**, 813–819 (2005).
48. M. Kucera *et al*., Reconstruction of sea-surface temperatures from assemblages of planktonic foraminifera: Multi-technique approach based on geographically constrained calibration data sets and its application to glacial Atlantic and Pacific Oceans. *Quat. Sci. Rev.* **24**, 951–998 (2005).
49. L. Jonkers, H. Hillebrand, M. Kucera, Global change drives modern plankton communities away from the pre-industrial state. *Nature* **570**, 372–375 (2019).
50. A. Menegotto, T. F. Rangel, Mapping knowledge gaps in marine diversity reveals a latitudinal gradient of missing species richness. *Nat. Commun.* **9**, 4713 (2018).
51. K. Block, T. Mauritsen, Forcing and feedback in the MPI-ESM-LR coupled model under abruptly quadrupled CO2. *J. Adv. Model. Earth Syst.* **5**, 676–691 (2013).
52. J. L. Dufresne *et al*., Climate change projections using the IPSL-CM5 Earth system model: From CMIP3 to CMIP5. *Clim. Dyn.* **40**, 2123–2165 (2013).
53. G. A. Schmidt *et al*., Configuration and assessment of the GISS ModelE2 contributions to the CMIP5 archive. *J. Adv. Model. Earth Syst.* **6**, 141–184 (2014).
54. J. P. Dunne *et al*., GFDL's ESM2 global coupled climate-carbon earth system models. Part I. Physical formulation and baseline simulation characteristics. *J. Clim.* **25**, 6646–6665 (2012).
55. M. A. Giorgetta *et al*., Climate and carbon cycle changes from 1850 to 2100 in MPI-ESM simulations for the coupled model intercomparison project phase 5. *J. Adv. Model. Earth Syst.* **5**, 572–597 (2013).
56. M. O. Hill, Diversity and evenness: A unifying notation and its consequences. *Ecology* **54**, 427–473 (1973).
57. A. Chao *et al*., An attribute-diversity approach to functional diversity, functional beta diversity, and related (dis)similarity measures. *Ecol. Monogr.* **89**, e01343 (2018).
58. A. Baselga, Partitioning the turnover and nestedness components of beta diversity. *Glob. Ecol. Biogeogr.* **19**, 134–143 (2010).
59. A. Baselga, The relationship between species replacement, dissimilarity derived from nestedness, and nestedness. *Glob. Ecol. Biogeogr.* **21**, 1223–1232 (2012).
60. R Core Team, *R: A Language and Environment for Statistical Computing* (R Foundation for Statistical Computing, Vienna, Austria, 2018).
61. J. Oksanen *et al*.,Vegan: Community Ecology Package. R Package Version 2.5-2. https://cran.r-project.org/web/packages/vegan/index.html. Accessed 3 May 2020.
62. A. Baselga, C. D. L. Orme, betapart: An R package for the study of beta diversity. *Methods Ecol. Evol.* **3**, 808–812 (2012).
63. S. N. Wood, *Generalized Additive Models: An Introduction with R* (CRC Press, Boca Raton, FL, ed. 2, 2017).
64. R. J. Hijmans, Raster: Geographic Data Analysis and Modeling. R Package Version 2.6-7. https://cran.r-project.org/web/packages/raster/index.html. Accessed 3 May 2020.
65. R. S. Bivand, E. Pebesma, V. Gomez-Rubio, *Applied Spatial Data Analysis with R* (Springer-Verlag, New York, NY, ed. 2, 2013).
66. H. Wickham, *ggplot2: Elegant Graphics for Data Analysis* (Springer-Verlag, New York, NY, 2016).
67. A. F. Zuur, *Mixed Effects Models and Extensions in Ecology with R* (Springer-Verlag, New York, NY, 2009).
68. J. M. Hoekstra *et al*., *The Atlas of Global Conservation: Changes, Challenges, and Opportunities to Make a Difference* (University of California Press, Berkeley, CA, 2010).